



Integrated Two-way Radar Backscatter Communication and Sensing with Low-power IoT Tags

Ryu Okubo rokubo2@illinois.edu University of Illinois at Urbana-Champaign Luke Jacobs lukedj2@illinois.edu University of Illinois at Urbana-Champaign Jinhua Wang lpkm3ex@virginia.edu University of Virginia

Steven Bowers sbowers@virginia.edu University of Virginia Elahe Soltanaghai elahe@illinois.edu University of Illinois at Urbana-Champaign

ABSTRACT

Integrated Sensing and Communication (ISAC) represents an innovative paradigm for enhancing spectrum and hardware utilization for both sensing and communication. A specific type of ISAC, radar backscatter communication, involves low-power nodes embedding data onto radar signal reflections rather than generating new signals. However, existing radar backscatter techniques only facilitate uplink communication from the tag to the radar, neglecting downlink communication. This paper introduces BiScatter, an integrated radar backscatter communication and sensing system that enables simultaneous uplink and downlink backscatter communication, radar sensing, and backscatter localization. This is achieved through the design of chirp-slope-shift-keying modulation on top of Frequency Modulated Continuous Wave (FMCW) radars, complemented by passive differential circuitry at the backscatter tags for low-power decoding. BiScatter also presents a packet structure compatible with off-the-shelf radars that offer accurate data processing and synchronization between radar and tag. We prototype this backscatter network in both 9GHz and 24GHz, demonstrating its capability to extend across different frequency bands. Our evaluations demonstrate that BiScatter supports two-way backscatter communication with BER lower than 10⁻³ up to 7m range and centimeter-level tag localization accuracy on top of off-the-shelf FMCW radars. The presented approach significantly augments the versatility and efficiency of ISAC for low-power devices.

CCS CONCEPTS

• Hardware → Digital signal processing; Wireless devices; Sensor devices and platforms; Wireless integrated network sensors.

KEYWORDS

Backscatter Communication, Integrated Sensing and Communication, mmWave backscattering, Two-way Communication, Radar Sensing



This work is licensed under a Creative Commons Attribution-NonCommercial-ShareAlike International 4.0 License.

ACM SIGCOMM '24, August 4–8, 2024, Sydney, NSW, Australia

© 2024 Copyright held by the owner/author(s).

**ACM ISBN 979-8-4007-0614-1/24/08*

https://doi.org/10.1145/3651890.3672226

ACM Reference Format:

Ryu Okubo, Luke Jacobs, Jinhua Wang, Steven Bowers, and Elahe Soltanaghai. 2024. Integrated Two-way Radar Backscatter Communication and Sensing with Low-power IoT Tags. In ACM SIGCOMM 2024 Conference (ACM SIGCOMM '24), August 4–8, 2024, Sydney, NSW, Australia. ACM, New York, NY, USA, 13 pages. https://doi.org/10.1145/3651890.3672226

1 INTRODUCTION

Integrated Sensing and Communication (ISAC) introduces a new approach for optimizing spectrum and hardware utilization for both sensing and communication. This design strategy not only cuts down device costs but also minimizes form factors and incorporates intelligence seamlessly into network infrastructures. One common type of ISAC is radar backscatter communication [26, 32], wherein a tag communicates information to radars by modulating and reflecting the radar signals, offering simultaneous support for low-power communication from the tag to the radar as well as accurate radar sensing. This could enable a wide range of new capabilities for radars embedded in phones [47], mixed-reality headsets [10], or small drones [19]. For example, consider a radar-equipped drone in a warehouse, leveraging the radar for simultaneous localization and mapping (SLAM) in low visibility but also simultaneously performing asset tracking or sending commands to passive backscatter tags (Figure 1). Such a system can significantly improve the battery life of industrial robots by integrating sensing, localization, and communication on top of the same radio unit.

Despite the above potential, existing radar backscatter communication systems have a major limitation: they predominantly focus on uplink communication or tag localization [32, 33, 37, 44], while overlooking downlink communication from the radar to tags. This limits the functionality of tags to read-only fiducial markers with no write access or configurability after deployment. A downlink connection from radar to tag can enable new opportunities, such as making on-demand retransmissions in case of packet loss, adapting the tag modulation scheme or data rate to link conditions, or minimizing interference. A recent work, called MilBack [29], targets this limitation by proposing a passive frequency scanning antenna (FSA) structure at the tag [17] and custom-built radar with two independent waveforms for downlink communication (two-tone signals) and uplink backscatter (FMCW signals). However, MilBack's design requires extra handshaking steps between the radar and tag to first localize the tag before establishing a downlink communication,

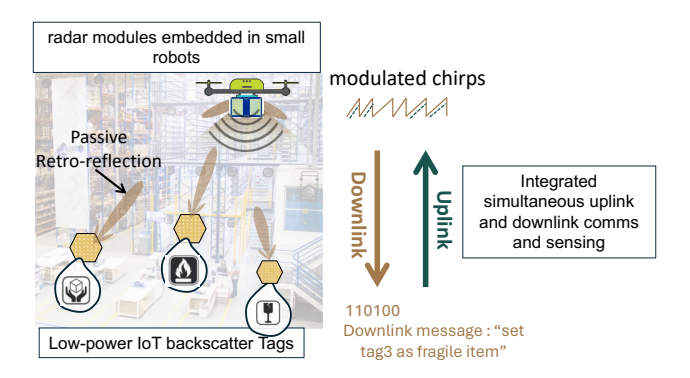


Figure 1: BiScatter provides an integrated two-way backscatter network and radar sensing between commercial radars and low-power backscatter nodes.

which could interfere with the primary functionality of radars in sensing. In addition, MilBack's custom-built waveform makes it incompatible with off-the-shelf radars, increasing hardware costs and complicating system integration. In contrast, radar-centric waveforms offer robustness and reliability by exploiting the inherent resilience of radar signals to interference and multipath effects.

In this paper, we introduce BiScatter¹, a fully integrated two-way radar backscatter communication and sensing system on top of off-the-shelf radars. BiScatter comprises a novel Chirp-Slope-Shift Keying (CSSK) modulation scheme that encodes bits into radar FMCW chirps for downlink communication by varying the chirp slope, a low-power backscatter tag design that enables simultaneous decoding of the radar signal and modulating the reflections for uplink communication, and an integrated decoding and localization algorithm at the radar. BiScatter's key innovation is the design of a low-power tag structure that leverages the unique shape of radar FMCW waveform to demodulate the radar data with a low-sampling ADC to preserve the tag's low-power consumption. This decoding scheme is independent of the radar's operating frequency and can be seamlessly extended to millimeter-wave bands. As such, our design makes three key contributions:

Low-power Two-way Tag Design: The first challenge is to develop a low-power backscatter tag that can enable two-way communication with an FMCW radar. The tag consists of three modules that all should operate in low-power mode and must be compatible with limited computational resources of backscatter tags: a decoder for receiving the radar signal and demodulating it; a modulator for uplink communication by modulating the amplitude or phase of received radar signal before reflecting it back; and a retro-reflector for redirecting the signal back toward the radar to compensate for high attenuation at higher frequencies such as millimeter-wave (mmWave) bands. To achieve this, BiScatter introduces a low-power baseband processing module at the tag that can estimate the radar chirp slopes using two delay lines of different lengths. Upon reception of the radar signal at the tag, the signal splits between two delay lines of different lengths and combines again at the end of the lines. Given the FMCW waveform of the radar, this results in a baseband beat frequency that is proportional to the chirp slope.

This enables a downlink communication from the radar to the tag by simply varying the radar chirp slopes. BiScatter integrates this decoding with passive retro-reflective Van Atta structures [44] with modulation for uplink communication.

Radar-Centric Two-way Communication: Another challenge is to design a radar modulation scheme that enables downlink data transmission from the radar while preserving radar's sensing capability. To achieve this, BiScatter introduces a Chirp-Slope-Shift Keying (CSSK) modulation scheme that creates multi-bit symbols by varying the FMCW chirp slopes. To maintain the radar range resolution, we fix the bandwidth of the chirps and control the chirp duration to modify the slope. As such, the downlink waveform can be generated by simply changing the radar chirp duration, making this modulation scheme compatible with off-the-shelf FMCW radars. We demonstrate that varying chirp slopes have minimal impact on radar localization and sensing functionalities by leveraging Fast-Fourier Transform (FFT) principles.

Integrated Radar Backscatter Communication and Sensing: Many perception systems, such as those in autonomous drones and robots, rely on continuous radar sensing for tracking or SLAM. So, the radar cannot afford to toggle between sensing and communication tasks. BiScatter addresses this challenge by introducing a fully integrated sensing and communication protocol that offers simultaneous operation of both modes while keeping each functionality transparent to the other ones. We propose a packet structure consisting of FMCW chirps with varying chirp slopes and inter-chirp delays that can carry not only the radar messages for downlink communication but also the tag modulation in the backscattered signal for uplink. The radar then uses the backscattered signal and the unique signature of the tag modulation to decode the tag message and accurately localize the tag.

Our system is built using off-the-shelf radars in two operating frequencies, 9GHz with 1GHz of bandwidth and 24GHz with 250MHz of bandwidth (conceptually, our system applies to 77GHz radar as well). We also custom-built BiScatter tags using low-power off-the-shelf components. Our evaluations across different settings demonstrate that BiScatter can achieve simultaneous uplink and downlink communication with a low bit error rate and centimeter-level localization accuracy while consuming only 48mW power, which is comparable with IoT power budgets and mmWave backscatter networks with only uplink support [32].

Contributions: Our technical contributions is summarized as:

- BiScatter is the first system design of a fully integrated radar backscatter communication and sensing that can achieve simultaneous uplink and downlink communication as well as radar sensing and localization.
- We present a radar modulation scheme, aka Chirp-Slope-Shift Keying (CSSK), that enables downlink communication between off-the-shelf radars and low-power backscatter tags while preserving radar's sensing capabilities.
- We introduce a two-way tag design that enables low-power downlink decoding through differential baseband processing, as well as backscatter modulation and retro-reflectivity for joint uplink communication and localization at the radar.
- BiScatter is implemented and evaluated with both sub-10GHz radars and commercial mmWave radars and is evaluated in several in-situ indoor scenarios.

 $[\]overline{{}^1\text{We}}$ chose the name BiScatter to convey the $\bf Bi$ directional radar backscatter feature of our system.

System	Uplink Comm	Downlink Comm	Tag Localization	Integrated Backscatter	Commercial Radar
				Sensing & Comms	Compatibility
Millimetro [44]	×	×	✓	X	✓
mmTag [32]	✓	×	×	X	✓
Milback [29]	✓	✓	✓	X	X
BiScatter (this work)	✓	√	√	✓	✓

Table 1: State-of-the-art radar backscatter system comparison

Ethics Statement: This paper does not raise any ethical concerns or issues.

2 BACKGROUND AND RELATED WORK

The related work can be divided to two groups: (a) Integrated Sensing and Communication (ISAC) systems (b) Radar Backscatter Communication. Table 1 provides a comparison between BiScatter and state-of-the-art ISAC and backscatter communication systems, highlighting the advantages of our approach.

2.1 Integrated Sensing and Communication

The sparsity of spectrum and bandwidth requirements has attracted researchers to combine wireless sensing and communication systems. As a result, previously competing sensing and communication operations are jointly optimized via a shared waveform and hardware platform. Most works in this domain either use radarcentric or communication-centric ISAC design, wherein the preexisting sensing or communication systems are used to enable the other functionality. For example, a large body of work on WiFi and cellular communication focuses on enabling sensing on top of ongoing communication [12, 24, 30, 41-43, 45, 46]. On the other hand, radar-centric ISAC systems focus on enabling communication between multiple radars with primarily sensing functionalities [16, 20, 28, 38]. More recent works on radar backscatter communication [7, 8, 13, 14, 23, 29, 31–34, 36, 37, 44, 50, 51] extend the scope of ISAC by allowing low-power backscatter tags actively communicate with radars. However, the existing radar backscatter systems only focus on uplink communication, in which the backscatter tag communicates with the radar by modulating the radar reflections. This limits the networking capability at the radar to read-only with no write access to the tag. BiScatter targets this limitation and proposes a radar backscatter communication system with both uplink and downlink communication with seamless integration of sensing and communication at the radar on top of off-the-shelf radars.

From the waveform design point of view, there are four main types of ISAC systems: (1) Utilizing independent waveforms for sensing and communication. For example, MilBack [29] leveraged two-tone signals for downlink communication and FMCW signals for sensing. However, such approaches still suffer from inefficient spectrum utilization. (2) Joint waveform design approaches that deploy dedicated dual-function waveforms [6, 9, 22]. These methods require custom radar development and active radios on both ends of communication links. As such, they are not suitable for low-power

IoT devices with limited computational resources. (3) Utilizing communication waveforms, such as orthogonal frequency-division multiplexing (OFDM), for sensing [24, 30, 46]. While these approaches enable ISAC between communication-centric devices, they are not compatible with radar systems. (4) Radar-centric approaches that embed digital messages into radar waveforms [40, 52]. The majority of these systems focus on enabling communication between high-power radars and are not applicable to low-power IoT devices such as backscatter tags. This paper falls under radar waveform-based ISAC systems, but unlike the previous works, it provides two-way communication between radar and passive backscatter tag. This enables a joint sensing and communication capability between off-the-shelf radars and low-power backscatter tags.

MilBack [29] is the closest previous work to this paper that offers two-way mmWave backscatter communication and localization. Milback uses a frequency scanning antenna at the tag with two modes of absorptive and reflective. In the absorptive mode, the tag receives the radar signal and passes it to a baseband processor for demodulation. However, due to the frequency selective beam pattern of the FSA structure, the radar first needs to estimate the orientation of the tag, which necessitates an extra handshaking process between the tag and radar before any communication or sensing. In addition, two independent waveforms are used for communication (a two-tone signal) and sensing (triangular FMCW chirps), which necessitates a custom-built access point with much higher power consumption compared to low-power off-the-shelf radars. It is worth noting that a radar-centric waveform compatible with off-the-shelf radars (e.g. FMCW automotive radars) can offer numerous advantages, including reduced costs, simplified integration, and enhanced system scalability. Leveraging established technology allows for faster deployment and scalability, particularly in critical applications like autonomous vehicles, where seamless coordination between sensing and communication is crucial, and the development timeline for custom radar designs to become widely available commercially spans 10+ years. BiScatter addresses these limitations by enabling simultaneous radar sensing and two-way backscatter communication with low-power tags on top of commodity radars while keeping each functionality transparent to the other.

2.2 Backscatter communication

The goal of backscatter communication is to enable low-power and battery-free objects with communication capabilities, either using specialized protocols such as RFID [48] or existing wireless networks, such as WiFi [5], LoRa [25], and FM Radios [49]. The availability of multi-GHz bandwidth in the mmWave frequency

range has attracted researchers to extend backscatter communication to mmWave on top of automotive radars [11]. Millimetro [44], Omniscatter [33], and hawkeye [8] provide cm-level tag localization accuracy using off-the-shelf radars, while mmTag [32] and MilBack [29] show feasibility of using mmWave backscatter for communication. Similar to BiScatter, MilBack extends backscatter communication to a two-way network, but it fails to utilize the spectrum effectively due to its usage of two independent waveforms for sensing and communication.

2.3 Preliminaries

In this section, we provide a short background on FMCW technology and Van Atta arrays, which will be used in the next sections to explain the BiScatter framework.

FMCW Waveform: Frequency Modulated Continuous Wave (FMCW) is one of the most widely adopted radar sensing technologies, using a continuous wave signal with linearly increasing frequency over time. This waveform is a frequency sweep, often referred to as a "chirp." As such, the transmitted radar signal can be modeled as:

$$s_t(t) = A_t \cos\left(2\pi \left(f_0 t + \alpha t^2\right)\right) \tag{1}$$

where A_t is the amplitude of the signal, f_0 is the starting frequency, and $\alpha = B/T_{chirp}$ is the frequency change rate, known as *chirp slope*. The slope of a chirp can be derived using its bandwidth (B) and chirp duration (T_{chirp}). The radar receives a delayed version of this signal reflected from objects in the environment, defined as:

$$s_r(t) = A_r \cos\left(2\pi \left(f_c(t-\tau) + \alpha(t-\tau)^2\right)\right) \tag{2}$$

where τ defines the time delay and is a function of the distance r between the radar and the target $r = \tau/2$. The received signal is then mixed with the transmitted signal, resulting in an Intermediate Frequency (IF) signal at a particular beat frequency (f_{IF}):

$$f_{IF} = \frac{2 \times \alpha \times r}{c} = \frac{2 \times r \times B}{c \times T_{chirp}}$$
 (3)

where c is the speed of light. Therefore, the range profile (e.g., distance of objects to the radar) can be defined using an FFT operation with a maximum unambiguous range estimate of

$$R_{max} = \frac{f_s c T_{chirp}}{2B} \tag{4}$$

where f_s represents the radar sampling frequency and a range resolution of

$$R_{res} = \frac{c}{2B} \tag{5}$$

Van Atta Array: The Van Atta array is a specialized antenna configuration designed for radar and communication systems, known for its unique capability to redirect Radio Frequency (RF) signals back towards the direction from which they arrived. The antenna elements of a Van Atta array are connected to transmission lines, which, in effect, makes each antenna element act as a phase-controlled reflector. When a signal is incident upon the array, the relative phase of each pair is adjusted dynamically to ensure that the reflected signals interfere constructively. As a result, the relative phase information due to the angle of arrival of the signals is preserved across the Van Atta array, resulting in retro-reflectivity. Recent mmWave backscatter communication systems [7, 32, 44] leverage

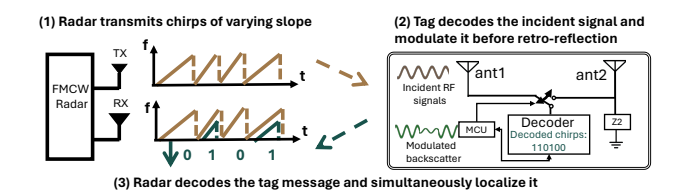


Figure 2: BiScatter System Overview

Van Atta arrays to create passive beam alignment between a low-power backscatter tag and mmWave radars. To provide uplink communication from the tag to the radar, the Van Atta arrays are populated with RF switches on their transmission lines to modulate the retro-reflections.

3 BISCATTER SYSTEM OVERVIEW

The proposed radar backscatter network includes an active radar and one or more backscatter nodes. The radar acts as an access point and uses Chirp-Slope-Shift Keying modulation to encode bits into FMCW signals by varying the chirp slope. This change in chirp slope serves as a communication symbol while preserving the radar's sensing capabilities. The other end of the communication link is one or more backscatter tags/nodes that are equipped with low-power differential circuitry that offers baseband processing to decode radar messages. This decoding module is integrated with a retro-reflective Van Atta structure that enables uplink communication by modulating the received radar signals before retroreflecting them. The retro-reflective feature of the tag boosts the SNR of backscattered signals to compensate for the high path loss of high-frequency radar signals. The radar then receives the modulated reflections from the tag and uses a super-resolution signal processing algorithm to detect the tag reflection and simultaneously localize the tag and decode its message.

Figure 2 shows a simple block diagram of BiScatter's tag architecture that comprises a pair of antennas connected to a transmission line. An RF switch is placed in the middle of the line, which toggles the Van Atta array between absorptive and reflective modes. When the RF switch is connected to the transmission line, the tag retro-reflects the signal. When it is connected to the decoder circuit with a 50 Ohm matched impedance, the radar signal from antenna 1 is absorbed and passed to the decoder. The other antenna gets terminated internally with the use of a non-reflective RF switch, thus creating the absorptive mode. With this structure, the tag can decode the downlink radar signals during the absorptive mode and modulate the backscatter signal for uplink as it switches between absorptive and reflective modes. Each of these components will be explained in subsequent sections in more detail.

3.1 Radar-Centric Downlink Communication

The downlink communication is defined from radar (aka access point) to the tag. We first define a modulation scheme at the radar that enables information coding without affecting the radar sensing and a corresponding packet structure that enables synchronization between the radar and the tag.

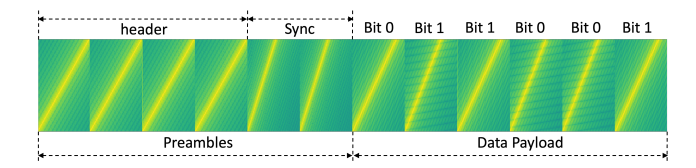


Figure 3: BiScatter Packet Structure. The preamble is used for finding the radar's chirp period and synchronization.

Radar Chirp-Slope-Shift-Keying Modulation: A radar modulation scheme can be defined by altering the FMCW waveform parameters such as bandwidth, chirp slope, or chirp rate. The core challenge is to preserve the radar sensing capabilities while communicating with the tag without requiring any custom hardware on the radar. As shown in Equations 4 and 5, changing these parameters could either affect the maximum unambiguous range detection (i.e., changing the chirp duration) or the range resolution (i.e. changing the bandwidth). Given the indoor use cases of BiScatter, we have more freedom in sacrificing the maximum range. Therefore, we leave the bandwidth intact in favor of range resolution and define a modulating scheme by altering the chirp duration. This effectively results in different chirp slopes representing downlink bits.

Downlink Packet Structure: We employ the traditional preamble+data payload packet structure, where the preamble includes a *header field* for detecting the chirp period and a *sync field* for synchronization and pointing the beginning of the data payload (shown in Figure 3). We allocate 2 unique chirp slopes for defining the header and sync fields in the preamble. BiScatter assumes a fixed chirp period T_{period} for the size of bit size, and it assumes that the maximum chirp duration cannot be larger than 80% of T_{period} . This assumption is defined based on minimum inter-chirp delay in commercial radars [18]. Therefore, for different chirp slopes, the inter-chirp delay should be adjusted accordingly to create the same bit size. Given the defined radar communication waveform, we next explain the tag structure for decoding the radar downlink messages.

3.2 BiScatter Tag Architecture

BiScatter enables two-way communication with an FMCW radar through interconnecting three modules: (1) a *decoder* for downlink communication that demodulates the received radar signals to extract the sent messages; (2) a *modulator* for uplink communication that modulates the radar signals before backscattering it by either altering amplitude, frequency, or phase of the received signal; and (3) a *retro-reflector* that compensates for high attenuation of backscattered signals in high frequencies especially mmWave bands by focusing the reflected power toward the radar.

One key challenge in designing these modules is the limited power budget and computational resources of backscatter nodes. The majority of commercial radars operate in mmWave frequency, which necessitates a GHz sampling rate using traditional demodulation algorithms. On the other hand, the typical approaches for creating directional communication (e.g., phased arrays) are too power-hungry to be used in backscatter nodes. Past works on mmWave backscatter communication leverage Van Atta structures combined with RF switches on the transmission line to enable

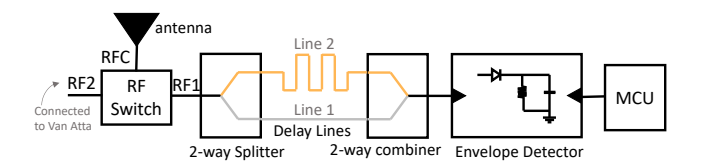


Figure 4: Tag Decoder Schematic

passive retro-reflectivity and backscatter modulation [32, 44], but none of these works provide downlink communication. A more recent work [29] proposes a frequency scanning antenna structure that enables integration of downlink, uplink, and localization in low-power backscatter nodes, but at the cost of using custom-built radars with independent waveforms for sensing and communication and extra handshaking steps between the tag and the radar. To address the above limitations, BiScatter's tag leverages a novel differential circuit with low-power baseband processing that can decode GHz FMCW signals with only a KHz-clocked ADC. We show that this decoding circuitry can be seamlessly integrated with (i) a Van Atta structure for passive retro-reflectivity and (ii) traditional backscatter modulation schemes for uplink communication.

3.2.1 **Tag Decoder**. During the absorptive mode of the tag, the signal received at antenna 1 (in Figure 2) will be sent to the decoder circuitry to demodulate the radar signals. The goal here is to estimate the chirp slopes through a low-power circuit and without any handshaking step between the tag and the radar. However, the challenge is that the decoding module should be hyper-sensitive to the linearly increasing frequency of FMCW waveforms. Previous work on LoRa backscatter demodulation [21] addressed this need by re-purposing the Surface Acoustic Wave (SAW) filters as a signal converter and leveraging the sharp frequency responses of SAW filters for decoding chirps. However, SAW filters typically operate in <1GHz frequency and are not applicable for radar backscatter systems, with the majority operating in mmWave bands. To address this challenge, BiScatter introduces a novel differential circuit that can estimate the chirp slopes with baseband processing by using two delay lines, shown in Figure 4. Upon reception of the radar signal at the decoder module, the signal splits between two delay lines with different lengths to create a controlled delay. At the end of the delay lines, the two delayed signals are combined together. Given the known expected delay between the two delay lines, we can then estimate a beat frequency by using an envelope detector with an internal low-pass filter. We show that this beat frequency is proportional to the chirp slope. Due to the small length difference between the two delay lines, the beat frequency will fall in the KHz range, which can be sampled using a low-power ADC.

This idea is inspired by the down-chirping operation at FMCW radars, which results in a beat frequency corresponding to the reflection time delay (refer to Section 2). The radar is able to estimate the distance to the object given the known chirp slope. The tag decoder uses a similar concept but with swapped known and unknown parameters: creating controlled and known delays to estimate the unknown radar chirp slopes. Similar to the down-chirping operation that enables the processing of a millimeter-wave signal

with a MHz-clocked ADC, our decoder structure enables estimating the chirp slopes using only a KHz-clocked ADC.

To formalize the expected beat frequency, let us define the incident signals at the end of the decoder's delay lines at time t. Without loss of generality and for ease of derivations, we assume a real radar. However, this technique works similarly for complex radars. The signal at the shorter delay line (line 1) can be represented as:

$$s_1(t) = A_t \cos\left(2\pi \left(f_0 t + \alpha t^2\right)\right) \tag{6}$$

where f_0 is the starting frequency of the radar chirps and α is the chirp slope. The signal at the end of the longer delay line (line 2) can be defined as

$$s_2(t) = A_t \cos\left(2\pi \left(f_0(t - \Delta T) + \alpha (t - \Delta T)^2\right)\right) \tag{7}$$

where ΔT is the time delay difference between the two lines. Signals 1 and 2 are combined using a second combiner that connects to the end of the delay lines, resulting in:

$$s_{combined}(t) = s_1(t) + s_2(t)$$
 (8)

Finally, the combined signal passes through an envelope detector, which measures the power of the received signal and also acts as a low-pass filter. The combination of the splitter and envelope detector is essentially equivalent to a mixer, which results in S_{IF} signal as

$$s_{IF}(t) = \cos\left(2\pi \left(f_0 \Delta T + \alpha t \Delta T - \alpha \Delta T^2\right)\right) \tag{9}$$

Within this output signal, the time-variant component is $\alpha t \Delta T$, where ΔT is the signal delay generated from the delay line difference. Given the FMCW waveform of the radar signal, this time delay corresponds to $\Delta T = \Delta f/\alpha$, which represents a direct linear relationship between chirp slope α and the so-called beat frequency Δf .

Delay Line Lengths: The next question is how much delay between the two delay lines is sufficient to create a measurable Δf . To answer this question, let us define ΔT based on the delay line properties as:

$$\Delta T = \frac{\Delta L}{kc} \tag{10}$$

where ΔL is the length difference of the two delay lines at the tag, and k is a constant factor related to the speed of EM signal in the delay line with respect to c, the speed of light. Combining equations 10 and the definition of chirp slope $\alpha = B/T_{chirp} = \Delta f/\Delta T$, we can calculate the beat frequency as:

$$\Delta f = \frac{B \times \Delta L}{T_{chirp} \times k \times c} \tag{11}$$

This equation shows the relationship between the expected frequency of the envelope detector output and four key parameters: radar bandwidth, chirp duration, cable length difference, and the dielectric constant of the delay lines. Among these parameters, we choose to alter the chirp duration to create different frequency components representing different radar symbols for downlink communication. For example, using a radar with 1GHz bandwidth, a delay-line length difference of 18inch with k value of 0.7 (for coax cables), we can alter the chirp duration between $T_{chirp_min} = 20us$ and 200us, which results in Δf ranging from approximately $\Delta f_{min} = 11k$ Hz to $\Delta f_{max} = 110k$ Hz. To measure Δf ,

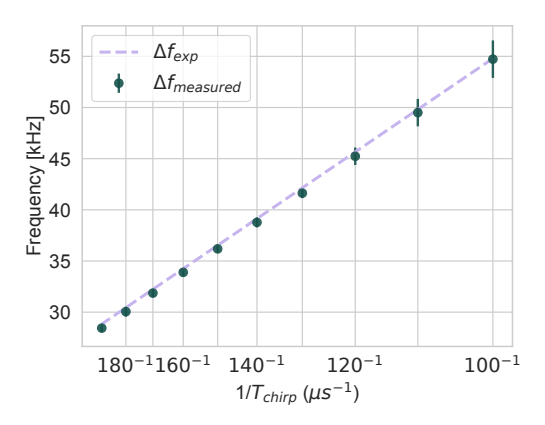


Figure 5: Benchmarking beat frequency Δf vs chirp duration T_{chirp}

the output of the envelop detector is connected to the ADC pin of a microcontroller with only a KHz sampling rate. This results in a simple, low-power, and low-cost decoder at the tag by only relying on two splitters, an envelope decoder, and a low-power processing unit.

It should be noted that the delay line difference ΔL should be selected carefully to create a large enough beat frequency range given the other parameters in equation 11. In addition, the equation assumes the dielectric constant of a delay line remains constant for the entire radar frequency range. However, this may not hold in practice, especially across a GHz bandwidth. To address this issue, it is a common practice to estimate the actual delay-line delay (ΔT) and the expected Δf per slope for a small frequency increment across the bandwidth as a one-time calibration. In the next section, we explain the processing algorithm at the tag to demodulate the downlink messages. We also elaborate on the delay-line design in the Implementation section.

Chirp-Slope-Shift-Keying Modulation Validation: To validate equation 11, we performed a controlled experiment by connecting a chirp generator (aka radar) to the tag decoder using wires. We fixed the bandwidth to 1GHz and the delay line difference to 45 inches; therefore, the chirp slope is the only parameter affecting the beat frequency of the envelope detector output. As shown in Figure 5, the beat frequency of the tag decoder shows a linear relationship with $1/T_{chirp}$, which matches with equation 11. The slope of this line corresponds to the other parameters in equation 11, which equals to $\frac{B \times \Delta L}{k \times c}$. A small deviation between the expected frequency and the measured value can be considered as the small difference in k, the speed of signal ratio with respect to the speed of light, which can be tuned with a one-time calibration.

3.2.2 Tag Decoding Algorithm. The tag samples the envelope detector output using an ADC. To find the corresponding beat frequency for each chirp slope, we can either use a sliding FFT or low-power filters such as the Goertzel algorithm [15] as a low-power point-by-point DFT evaluator. However, there are several practical challenges that BiScatter tag has to deal with. First, the FMCW radars usually incorporate inter-chirp delays between different sweeps for facilitating down-chirp operation [18]. These

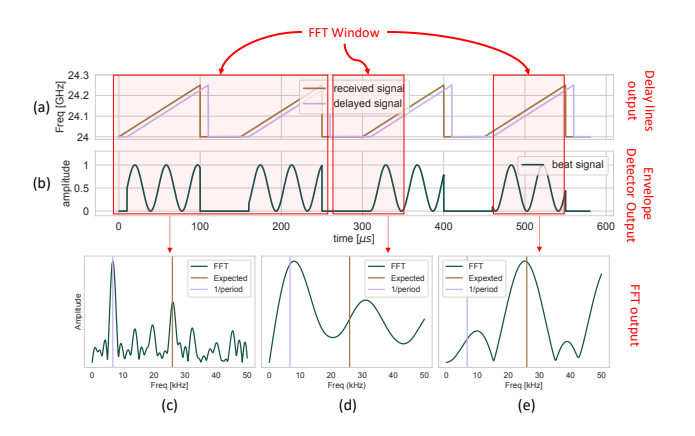


Figure 6: The radar inter-chirp delays impose constraints on the tag's decoder in finding the right FFT window size and window alignment to extract the beat frequency.

inter-chirp delays impose some constraints on FFT window size and the sliding FFT operation. To explain this effect, consider the three scenarios illustrated in Figure 6. Figure 6(a) shows the frequency domain signals at the end of the two delay lines, Figure 6(b) shows the time domain sampled data after the envelope detector, and Figures 6(c-e) shows the corresponding FFT outputs for the highlighted FFT windows. Figure 6(c) shows an FFT output for a window size larger than a chirp. In this case, the chirp frequency rate will also show up in the FFT output, which can cause ambiguity in finding the right beat frequency. Figure 6(d) shows a scenario where a chirp-long FFT window size is used, but there is a misalignment between the FFT window and the chirp due to interchirp delays, causing errors in beat frequency estimates. Figure 6(e) shows the ideal scenario where the FFT window size is smaller than a chirp period, and it is aligned with a chirp. Note that the chirp period $T_{period} = T_{chirp} + T_{interC}$, where T_{interC} defines the interchirp delay. To address these challenges, we leverage the proposed packet structure in Section 3.1 to find the correct window size. The tag first performs an FFT across multiple header bits (similar to the case in Figure 6(c)) by defining a large FFT window. This allows the tag to estimate the chirp period T_{period} to then determine the proper FFT window size for decoding the data payload. The tag then performs a sliding FFT with the estimated window size over the preamble to identify the sync bits and synchronize the data payload for decoding. It is noteworthy that adjusting the inter-chirp delay does not impact the corresponding beat frequency of each radar symbol, as it is analogous to padding zeros for FFT.

Downlink Data Rate: The radar symbol size can be defined using the minimum and maximum chirp duration, as well as the minimum interval between beat frequencies defined based on the tag noise floor:

$$N_{symbol} = \log_2(N_{slope}) \tag{12}$$

$$N_{slope} = \frac{(\Delta f_{\text{max}} - \Delta f_{\text{min}})}{\Delta f_{int}}$$
 (13)

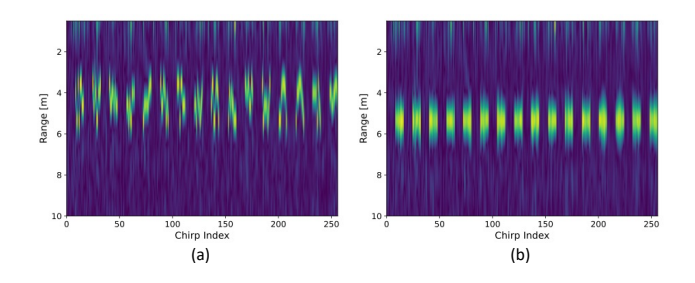


Figure 7: Varying chirp slopes within a frame causes ambiguity in radar range-profile (a), which are addressed in BiScatter's ISAC protocol (b).

where N_{symbol} denotes the number of bits in a radar symbol and N_{slope} defines the number of chirp slopes. $\min_{\Delta f}$ and $\max_{\Delta f}$ are the corresponding minimum and maximum beat frequencies defined by the maximum and minimum chirp durations, respectively. Δf_{int} denotes the interval between every two beat frequencies that is defined empirically based on the tag noise floor. Therefore, the achievable downlink data rate can be calculated using the equation below:

$$data_rate = \frac{N_{symbol}}{T_{period}}$$
 (14)

To increase the data rate, we need to either decrease the period of one symbol or increase the number of bits per symbol. For example, with a symbol size of 10 bits (i.e. $2^{10} + 2$ distinctive chirp slopes) and a chirp period of $100 \, \mu s$, we can achieve .1Mbps downlink data rate, which is sufficient for sending commands to the tag such as assigning the uplink modulation frequency.

3.2.3 **Tag Retro-reflector and Modulator**. For uplink communication, the tag uses an RF switch on the Van Atta transmission line to modulate the received radar signals before retro-reflecting them back to the radar. The switching rate of the RF switch defines the modulation frequency and the duty cycle pattern. The radar uses this information to decode the tag message and simultaneously localize the tag, which is explained in the next section.

3.3 BiScatter ISAC Protocol

The previous section presented the radar downlink mechanism and tag architecture to decode the downlink messages and modulate the reflections for uplink communication. In this section, we explain how this two-way communication can be integrated with radar sensing. BiScatter's goal is to make each of these operations transparent to the others so the radar can seamlessly transmit and receive messages while also performing its primary sensing operation. However, the challenge is that the radar downlink data payload includes a sequence of chirps with different slopes. The radar receives the reflection of these chirps from the environment as well as the tag and performs down-chirping to extract the IF signals to detect and locate the tag while performing other sensing tasks. However, the challenge is that the IF frequency is a function of chirp duration, as shown in equation 3. Therefore, the chirpslope-shift-keying modulation for uplink communication results in varying IF frequencies across chirps with varying slopes, causing ambiguity in interpreting the range profile. Figure 7(a) shows a range profile example for a frame with a modulating tag while the radar is also sending uplink communication. We can see that the range readings are inconsistent across chirps despite the tag being static.

To address this issue, BiScatter first converts each FFT bin to its corresponding range using equation 3. This filters out the IF frequency variations by accounting for the chirp duration changes (note the multiplication of f_{IF} and T_{chirp}). However, the range bin intervals are still different for each chirp, causing a misalignment problem when combining multiple chirps for Doppler measurements or other sensing applications. This is because the maximum unambiguous range that the radar can detect is determined by chirp duration (shown in Equation 4). Accordingly, the corresponding range interval of each FFT bin can be modeled as

$$range[n] = \frac{n}{N_{FFT}} R_{max}$$
 (15)

where n defines the FFT bin number with $n = \{1, 2, 3, ..., N_{FFT}\}$, and N_{FFT} defines the total number of FFT bins. As such, range[n] is expected to be different for different chirp slopes. To overcome this challenge, we use pairwise interpolation between every two FFT bins and rescale the range profile to align the range profile of different chirp slopes. Figure 7(b) shows the range profile after the IF correction.

Tag Localization and Uplink Decoding: After the above IF correction, the radar can simultaneously decode the uplink messages from the tag and localize the tag using the range-Doppler profile. BiScatter uses the first chirp of each frame for background subtraction. This allows us to eliminate strong multipath reflections and background noise from the environment. BiScatter then uses the well-known range-Doppler processing proposed in previous works [7, 32, 44] to first localize the tag based on its expected modulation frequency and then decode the message. The key insight is that the tag modulation across chirps appears as a square wave multiplied by the tag's corresponding IF signal. Therefore, the second FFT across chirps converts the tag modulation into a sinc function where the primary frequency component equals the modulation frequency. BiScatter then uses the matched filtering proposed in previous works [44] to find the tag signature for localization. It should be noted that BiScatter's structure is compatible with different backscatter modulation schemes such as On-Off keying, Amplitude Shift Keying (ASK) or Frequency Shift Keying (FSK) modulation, which can be developed on top of the tag's RF switch.

4 IMPLEMENTATION

BiScatter radar: We evaluated BiScatter using off-the-shelf FMCW radars in two different frequencies of 9GHz and 24GHz. It is important to note that our system's functionality is not contingent on the specific frequency range but rather relies on the bandwidth of the FMCW signal. Hence, the main goal of selecting these two radars is to test the effect of bandwidth. The 9GHz radar offers flexible bandwidth configuration and chirp-level slope adjustment, for which we used a Texas Instruments LMX2492EVM chirp generator and a ZX80-05113LN+ amplifier, resulting in a maximum power output of 7dBm. For mmWave radar, we use Analog Devices

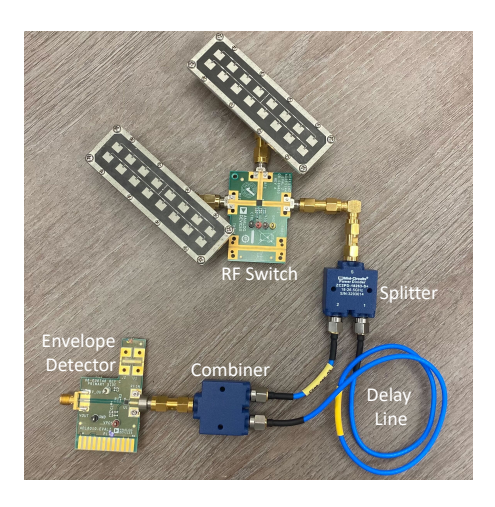


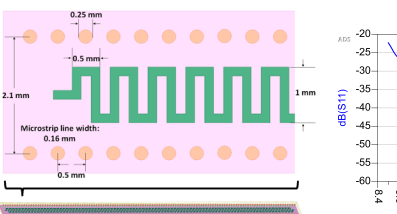
Figure 8: BiScatter Tag Prototypes

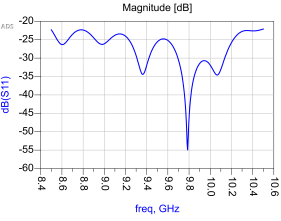
TinyRad [1], operating at 24GHz with 250MHz bandwidth and a maximum power output of 8 dBm.

BiScatter Backscatter node: Figure 8 shows the prototype of our proposed tag. We implemented the node using off-the-shelf circuit components such as ADRF5144 SPDT RF switch [3], two ZC2PD-18263-S+ splitters/combiners [4] at the two ends of delay lines, and one ADL6010Evalz envelope detector [2] for detecting the beat frequency of the chirp slopes. The antennas are connected to RFC and RF1 ports of the switch, creating a 2-element van Atta Array, while RF2 is connected to the decoding module for downlink communication.

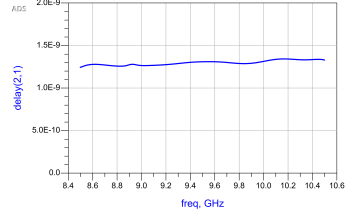
We also designed the delay lines for the tag decoder using ANSYS HFSS software. As shown in Figure 9, we use microstrip meander lines [39, 53] that offer controlled delay to electromagnetic signals in a space-efficient manner. The line is characterized by its meandering pattern, a key feature responsible for extending the electrical length of the transmission path. As the electromagnetic wave travels along this extended, meandering path, it experiences a longer transit time than a straight line of equivalent physical length, resulting in the desired delay in a compact form factor. The design and implementation require careful consideration of the line's geometry, the width of the conducting strip, the dielectric properties of the substrate, and the overall layout. Figures 10-11 show the performance of the designed line in 9GHz spanning a 1GHz bandwidth. In this design, we used Rogers 3006 as the dielectric material and were able to achieve 1.26ns of delay across the 1GHz bandwidth with overall delay line dimensions of 64 mm x 3mm x 0.5 mm.

At mmWave frequencies (e.g. 24 GHz), the substrate dielectric constant critically influences microstrip meander line performance, affecting impedance, delay time, and miniaturization. Increased dielectric constant values can facilitate longer delay time and smaller component sizes but may introduce increased dielectric losses, which are crucial at mmWave frequencies. These factors necessitate careful material selection and design optimization to balance the benefits and drawbacks posed by the dielectric constant in higher frequencies.









lay Line

Figure 9: PCB Integrated De- Figure 10: S11 parameters of the PCB delay line

Figure 11: The measured insertion loss and delay across the line's frequency range

4.1 Power Consumption

The main components needed at the tag are an RF switch, an envelope detector, and an MCU or FFT processor. We break down the tag power consumption into two operating modes of (1) Continuous communication-and-sensing mode, where the tag is constantly decoding any received signal, (2) Sequential uplink/downlink mode, where the radar uses the preamble to define the write vs. read modes.

Continuous Communication and Sensing Mode: In simultaneous and continuous uplink/downlink operation, all components are active constantly, with the RF switch and envelope detector consuming 2.86 µW and 8 mW, respectively. To optimize MCU power consumption, we investigated the impact of reducing the clock cycle, setting a clock frequency of 1 MHz to meet the required ADC sampling speed. Under this configuration, the typical MCU power consumption is approximately 40 mW, resulting in a total system power consumption of approximately 48 mW. We anticipate that this power consumption can be reduced in a custom IC design. It is a common practice to adapt a prototype design into a custom IC design after prototype validation to achieve the lowest possible power consumption. We predict that the power consumption can be reduced to as low as 4mW by integrating a MOSFET switch, an operational amplifier (op-amp) for envelope detection, and a lowpower ADC based on Walden's Figure of Merit (FoM). Additionally, replacing the FFT with the Goertzel filter, a point-by-point DFT evaluator, on the MCU can reduce power usage since evaluating the entire FFT spectrum is not necessary. In addition, recent advancements in low-power FFT processors present further opportunities for power reduction.[27, 35, 54]

Sequential Uplink/Downlink Mode: For use cases where simultaneous communication and sensing are not required, the power can be further reduced by alternating between uplink and downlink communication. By strategically employing sleep mode for the MCU during uplink intervals, substantial power savings can be achieved as the MCU enters an ultra-low power state during its sleep mode. In this mode, the RF switch can be activated using the PWM signal requiring less than $3\,\mu\text{W}$ to operate. We emphasize the importance of tuning the downlink/uplink frequency to optimize the tag's overall power consumption further.

5 **EVALUATION**

We evaluate BiScatter's performance in an indoor office space with substantial multipath propagation. The tag is positioned at different

locations relative to the radar in distances from .5m to 7m. We first test the impact of different radar waveform parameters, such as bandwidth, chirp duration, or symbol size, as well as the impact of tag configuration, such as the delay line length. We used the 9GHz chirp generator for all of these experiments unless it is mentioned for its full configurability. In each experiment, we fix the chirp period to 120us, and 10000 frames are collected for each setup. We run a calibration at 0.5m distance, and used the same calibration configuration for all the other experimental setups. For evaluating the localization performance, we use the 1D-ranging performance, where the ground truth was collected using BOSCH laser distance meter. finally, we show the generalizability of the tag structure to off-the-shelf radars and mmWave frequency range by comparing the system performance in 24GHz using Analog Devices radar.

Two-Way Communication Performance

In this section, BiScatter's downlink performance over different radar or tag parameters is evaluated. It is worth mentioning that the maximum downlink data rate is a function of several parameters, such as symbol size and chirp duration (equation 14), while the symbol size itself is a function of radar bandwidth, delay-line length difference, and range of chirp durations at the radar. As such, we show the impact of each parameter on Bit-Error-Rate (BER) while isolating the rest of the parameters, which also indirectly represents the downlink data rate.

Impact of Radar Symbol Size on Downlink Performance: We first show how radar symbol size affects the BER of the tag. As mentioned in section 5, BiScatter is able to encode different numbers of bits in each chirp slope to increase the data rate at the cost of decreasing the spacing between different chirp slopes

representing the symbols. Figure 12 shows the BER over different symbol sizes for three different radar bandwidths. We can see that BiScatter can achieve BER of $< 10^{-3}$ with 1GHz bandwidth and 5 bits per symbol, but the error rate degrades for smaller bandwidths or larger symbol sizes. This is due to a smaller gap between beat frequencies, causing ambiguity in decoding and an increased Bit

Impact of Radar-tag Distance on Downlink Performance:

We also evaluate the performance of BiScatter's downlink over different Signal to Noise Ratio (SNR). In this experiment, we position the tag in front of the radar while changing the distance, which results in different SNRs. We evaluated the Bit Error Rate performance of the tag decoder for different maximum bounds on downlink data rates, which is achieved by changing the symbol size. It should be

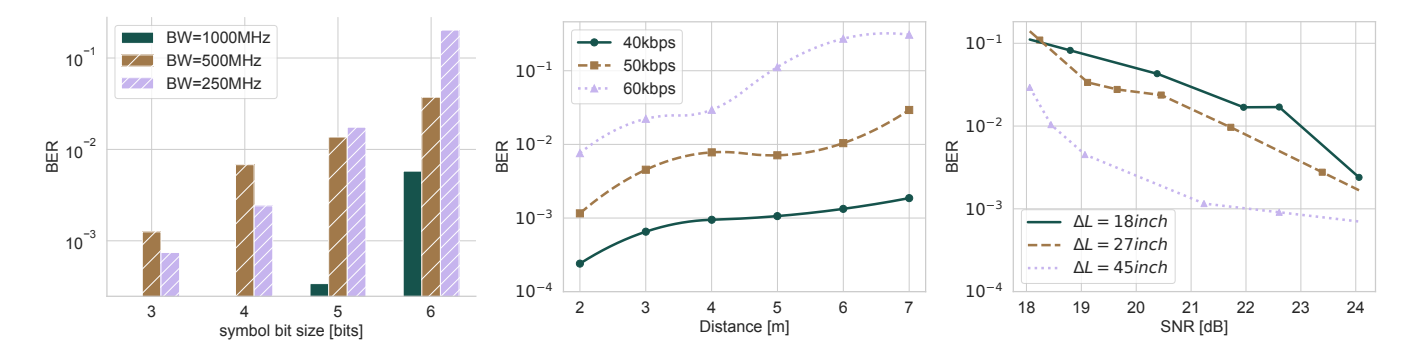


Figure 12: Downlink BER vs. Symbol size: BiScatter can achieve higher performance for larger bandwidths, especially for larger symbol sizes.

Figure 13: Downlink BER vs. Distance: BiScatter can maintain a low BER for over 7m distance with the equivalent of 16db SNR

Figure 14: Downlink BER vs. SNR: BiScatter can be improved at lower SNRs by increasing the tag's delay-line length difference.

noted that the symbol sizes are a function of the bandwidth and delay-line length difference, so for these experiments, we change the delay-line length differences while keeping the bandwidth fixed at 1GHz. Figure 13 shows the result of BER vs distance. We can see that BiScatter can maintain a low BER across different SNRs and up to 7m range. The error rate increases for higher symbol sizes. So, to achieve a larger symbol size at longer distances, a larger bandwidth or longer delay line is desirable to create more separation between beat frequencies of different radar chirp slopes.

Impact of Tag Delay-Line on Downlink Performance: To show the impact of delay lines, next, we evaluate the bit error rate over SNR for different ΔL or length differences between the two delay lines at the tag. In these experiments, we isolate the effect of symbol size by assuming a fixed size of 5 bits across all experiments and a fixed bandwidth of 1GHz. Figure 14 shows the result of BER over SNR for different cable lengths with a fixed symbol size of 5 bits. The error rate increases for the smaller cable lengths, as the separation between beat frequencies decreases. As mentioned in the previous section, a longer delay line is desirable to ensure lower BER. However, that could result in a larger tag form factor and require more tag design iterations to achieve a constant delay across the radar bandwidth.

Uplink Performance: BiScatter uses the welknown backscatter modulation techniques used in previous works [44] for uplink communication. Based on the previous evaluations, the main factor affecting the uplink performance from the tag to the radar is the SNR of two-way backscatter link and distance. As shown in Figure 15, the SNR drops as the distance increases; however, we are still able to get over 4dB SNR at 7m. This corresponds to a theoretical BER of 1e-2 assuming a simple on-off-keying modulation, which we consider to be sufficient for practical use cases. This is mainly due to retro-reflective behavior of the tag that preserves the high SNR even at longer ranges. It should be noted that the SNR range of the uplink is significantly lower than the downlink due to the round-trip nature of backscatter signals. Hence, the signal undergoes double attenuation in the uplink compared to the downlink. Note that the uplink data rate is limited by the switching speed of the tag switch and the maximum chirp duration. One can increase

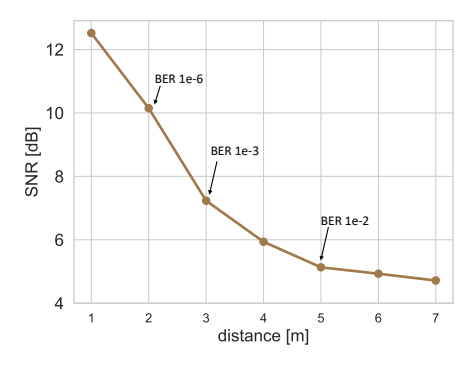
the switching rate by using a smaller range of chirp durations to increase the uplink data rate.

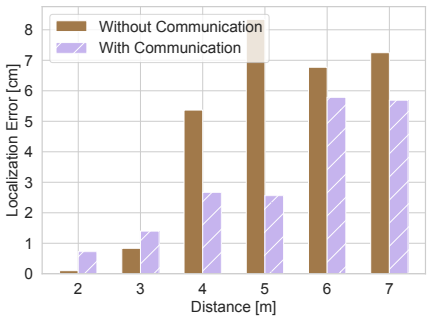
5.2 Tag Localization Performance

Finally, we evaluate the radar's tag localization performance under two different scenarios: (1) where the radar is using a fixed chirp slope with the goal of sensing only or simultaneous sensing and uplink communication, (2) where the radar performs integrated two-way backscatter communication and sensing by altering the chirp slopes within a frame for downlink communication. As shown in figure 16, the downlink communication of the radar has a minimal impact on the localization performance of the tag and BiScatter can preserve the centimeter-level accuracy for tag localization; in fact, in most cases, the localization error is lower during communication. This shows that the varying chirp slopes can offer diversity to filter out noise. In addition, this demonstrates the effectiveness of BiScatter's IF frequency correction algorithm to account for varying maximum unambiguous range as the radar alters the chirp duration for downlink communication.

5.3 Extension to Millimeter-wave Frequency

BiScatter tag framework can be seamlessly extended across different frequencies including millimeter-wave as the ADC sampling rate is independent of the radar operating frequency. To show this, we evaluate the BiScatter performance over two radars operating in two different frequencies of 9GHz and 24GHz. To perform a fair comparison, we set the bandwidth in both radars to 250MHz, constrained by the maximum available ISB band in 24GHz. Figure 17 compares the downlink Bit Error Rate (BER) of two radars over different Signal-to-Noise Ratios (SNR) with every other parameter fixed. We alter the SNR by changing the distance between the tag and the radar. As the results show, we have a comparable bit error rate between 9GHz and 24GHz radar experiments. The slightly better performance of 24GHz radar is due to a higher quality clock and signal generator. It should be noted that the higher path loss of RF signals in 24GHz causes the same SNR to be achieved at different distances for the two radars. However, a higher gain antenna can





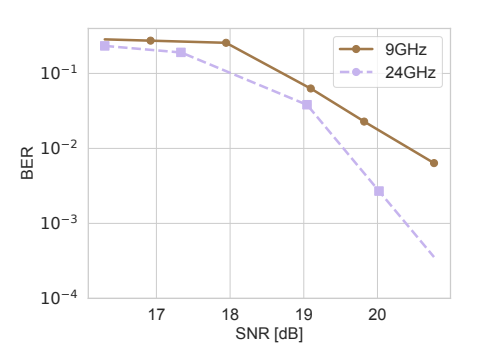


Figure 15: Uplink SNR vs. Distance: the tag retro-reflective structure provides high SNR even at longer distances to preserve the low bit error rate.

Figure 16: BiScatter can maintain high localization accuracy even at the presence of two-way communication with varying chirp slopes

Figure 17: BiScatter provides a comparable performance across frequencies including mmWave bands.

be used in 24GHz, given the smaller wavelength and antenna form factor.

6 DISCUSSIONS

In the previous section, we demonstrated the robustness of BiScatter's downlink, uplink, and integrated operation in different scenarios as well as the impact of different parameters on BiScatter's performance. BiScatter is a natural solution for integrated two-way communication and sensing between off-the-shelf radars and low-power IoT devices. Nevertheless, BiScatter still has some limitations, and there are a few unaddressed avenues for future improvements:

Radar Downlink Data-Rate: As mentioned in section 5, BiScatter's data rate is a function of minimum chirp duration in commercial radars $(T_{chirp\ min})$ and the number of slopes (N_{slope}) . The key limiting factor here is that commercial FMCW radars can only support a minimum of 10 - 20us chirp duration, imposed by the radar sampling rate. On the other hand, the number of slopes only grows the data rate logarithmically, which is not an efficient way of increasing the data rate. There is also a trade-off between larger N_{slope} and BER, which is shown in previous evaluations. As a result, the current data rate of BiScatter is limited to 50-100kbps. Nevertheless, This data rate is comparable to RFID and LoRA downlink data rates but offers a portable reader setup based on commercial radars. This data rate is sufficient for sending commands to low-power tags, or broadcasting a message for synchronization purposes. In future work, more complex downlink modulations based on chirp-spread-spectrum (CSS) can be used to improve the

Radar Downlink Operating Range: The current version of BiScatter can reliably operate up to 7m as the downlink bit error rate degrades for larger distances. A notable limitation contributing to this operational constraint is the elevated insertion loss and noise floor of the tag decoder. Various components in the tag decoder contribute to the overall tag's insertion loss, such as splitters/combiners, delay lines, and connectors. Additionally, the noise floor of the envelope detector serves as another factor restricting the operational range. The tag circuitry can be improved in future work by using

analog circuitry and eliminating connectors to achieve longer-range operation.

Delay-line Length: As shown in the previous section, the delay-line length at the tag plays an important role in trading off between the downlink data rate (by increasing the delay line length) and operating range (by increasing the insertion loss for longer lines). In addition, the longer delay lines suffer from non-linear phase shift across the entire radar bandwidth. The between-line coupling also becomes more significant in the mmWave frequency range, potentially leading to interference and compromised signal integrity. To address these challenges, more advanced delay-line design, such as combining the meander lines with stubs or pairing two transmission lines to create constructive coupling, is needed.

Extension to Multi-Radar Multi-Tag Scenarios: In this paper, we mainly focused on a downlink design that is compatible with commercial radars and the design of an integrated sensing and communication protocol on top of commodity radars. The current version can be seamlessly extended for broadcast communication between a single radar and multiple tags or simultaneous multitag communication by assigning unique modulation frequencies per tag for uplink communication and incorporating tag ID in the downlink header. In addition, slotted aloha and similar time division multiplexing techniques can be used for extending the proposed system to multi-radar scenarios. Exploring the trade-off between maximum data rate per node vs. overall network throughput is an interesting avenue to be explored in the future.

BiScatter's Potential Applications: BiScatter enables a two-way backscatter communication as well as simultaneous sensing and localization using an off-the-shelf radar and a custom-built backscatter tag. The biggest advantage of such system is the write access for radar to configure the tags, broadcast messages for waking up the tags. This is superficially useful in autonomous applications that radars are widely used for tracking and sensing purposes. For example, a drone setting up a new tag as spatial feature while performing obstacle detection using the on-board radar. In addition, BiScatter enables transparent communication and sensing, in which the two-way communication with a tag has no impact on primary applications of radars for sensing. For example, BiScatter can enable

real-time, bidirectional communication between the vehicle and its environment, providing continuous updates on path conditions, traffic, and potential hazards.

7 CONCLUSION AND FUTURE WORK

This paper presents BiScatter, a unified system for integrated radar backscatter communication and sensing, facilitating simultaneous uplink, downlink, radar sensing, and localization functionalities. This achievement is realized by designing novel chirp-slope-shift-keying modulation on top of FMCW radars. Additionally, the system incorporates low-power differential circuitry at the backscatter nodes to ensure efficient decoding processes. Through implementation and evaluation in an indoor environment, our system demonstrated a Bit Error Rate (BER) of less than 10^{-3} and achieved centimeter-scale localization accuracy within a specified range of up to 7 meters. BiScatter emerges as a comprehensive solution for simultaneous communication and sensing applications, such as those pertinent to indoor robots.

ACKNOWLEDGMENT

We thank our reviewers and shepherd for their insightful feedback which helped improve this paper. We also thank Wireless, Sensing, & Embedded Networked Systems (iSENS) Lab group members at the University of Illinois Urbana-Champaign for their inputs.

REFERENCES

- 2020. Analog Devices TinyRad. https://www.analog.com/media/en/technical-documentation/user-guides/ev-tinyrad24g-ug-1709.pdf.
- [2] 2024. Analog Devices Envelope Detector. https://www.analog.com/en/resources/ evaluation-hardware-and-software/evaluation-boards-kits/eval-adl6010.html.
- [3] 2024. Analog Devices SPDT Switch. https://www.analog.com/en/products/ adrf5144.html.
- [4] 2024. Mini-Circuits 2-way splitter. https://www.minicircuits.com/pdfs/ZC2PD-18263-S+.pdf.
- [5] Ali Abedi, Farzan Dehbashi, Mohammad Hossein Mazaheri, Omid Abari, and Tim Brecht. 2020. WiTAG: Seamless WiFi Backscatter Communication. In Proceedings of the Annual Conference of the ACM Special Interest Group on Data Communication on the Applications, Technologies, Architectures, and Protocols for Computer Communication (Virtual Event, USA) (SIGCOMM '20). Association for Computing Machinery, New York, NY, USA, 240–252. https://doi.org/10.1145/3387514.3405866
- [6] Mohammad Alaee-Kerahroodi, Ehsan Raei, Sumit Kumar, and Bhavani Shankar M. R. R. 2022. Cognitive Radar Waveform Design and Prototype for Coexistence With Communications. *IEEE Sensors Journal* 22, 10 (2022), 9787–9802. https://doi.org/10.1109/JSEN.2022.3163548
- [7] Kang Min Bae, Namjo Ahn, Yoon Chae, Parth Pathak, Sung-Min Sohn, and Song Min Kim. 2022. OmniScatter: extreme sensitivity mmWave backscattering using commodity FMCW radar. In Proceedings of the 20th Annual International Conference on Mobile Systems, Applications and Services. 316–329.
- [8] Kang Min Bae, Hankyeol Moon, Sung-Min Sohn, and Song Min Kim. 2023. Hawkeye: Hectometer-range Subcentimeter Localization for Large-scale mmWave Backscatter. In Proceedings of the 21st Annual International Conference on Mobile Systems, Applications and Services. 303–316.
- [9] Ahmad Bazzi and Marwa Chafii. 2023. On Integrated Sensing and Communication Waveforms With Tunable PAPR. IEEE Transactions on Wireless Communications 22, 11 (2023), 7345–7360. https://doi.org/10.1109/TWC.2023.3250263
- [10] Tara Boroushaki, Maisy Lam, Laura Dodds, Aline Eid, and Fadel Adib. 2023. Augmenting Augmented Reality with {Non-Line-of-Sight} Perception. In 20th USENIX Symposium on Networked Systems Design and Implementation (NSDI 23). 1341–1358.
- [11] Xiuzhang Cai. [n. d.]. Autonomous Vehicles: MMW Radar Backscattering Modeling of Traffic Environment, Vehicular Communication Modeling, and Antenna Designs. http://deepblue.lib.umich.edu/handle/2027.42/163001 Accepted: 2020-10-04T23:26:31Z.
- [12] Francesco Calabrese, Laura Ferrari, and Vincent D Blondel. 2014. Urban sensing using mobile phone network data: a survey of research. Acm computing surveys (csur) 47, 2 (2014), 1–20.

- [13] Jessica Centers and Jeffrey Krolik. 2022. Vibrational radar backscatter communication using resonant transponding surfaces. In 2022 IEEE 12th Sensor Array and Multichannel Signal Processing Workshop (SAM). IEEE, 71–75.
- [14] Weilin Chen. 2023. Survey of Millimeter Wave Backscatter Communition Systems. arXiv preprint arXiv:2305.10302 (2023).
- [15] Joe F Chicharo and Mehdi T Kilani. 1996. A sliding Goertzel algorithm. Signal Processing 52, 3 (1996), 283–297.
- [16] Alex R Chiriyath, Bryan Paul, and Daniel W Bliss. 2017. Radar-communications convergence: Coexistence, cooperation, and co-design. *IEEE Transactions on Cognitive Communications and Networking* 3, 1 (2017), 1–12.
- [17] Magnus Danielsen and Rolf Jorgensen. 1979. Frequency scanning microstrip antennas. IEEE Transactions on Antennas and Propagation 27, 2 (1979), 146–150.
- [18] Vivek Dham. 2017. Programming chirp parameters in TI radar devices. Application Report SWRA553, Texas Instruments 1457 (2017).
- [19] Sedat Dogru and Lino Marques. 2020. Pursuing drones with drones using millimeter wave radar. IEEE Robotics and Automation Letters 5, 3 (2020), 4156–4163.
- [20] Zhiyong Feng, Zixi Fang, Zhiqing Wei, Xu Chen, Zhi Quan, and Danna Ji. 2020. Joint radar and communication: A survey. China Communications 17, 1 (2020), 1–27.
- [21] Xiuzhen Guo, Longfei Shangguan, Yuan He, Nan Jing, Jiacheng Zhang, Haotian Jiang, and Yunhao Liu. 2022. Saiyan: Design and Implementation of a Low-power Demodulator for LoRa Backscatter Systems. In 19th USENIX Symposium on Networked Systems Design and Implementation (NSDI 22). USENIX Association, Renton, WA, 437–451. https://www.usenix.org/conference/nsdi22/presentation/guo
- [22] Aboulnasr Hassanien, Moeness G Amin, Elias Aboutanios, and Braham Himed. 2019. Dual-function radar communication systems: A solution to the spectrum congestion problem. *IEEE Signal Processing Magazine* 36, 5 (2019), 115–126.
- [23] Thomas Horton King, Jizheng He, Chun-Kai Yao, Akarsh Prabhakara, Mohamad Alipour, Swarun Kumar, Anthony Rowe, and Elahe Soltanaghai. 2023. Platypus: Sub-mm Micro-Displacement Sensing with Passive Millimeter-wave Tags As" Phase Carriers". In Proceedings of the 22nd International Conference on Information Processing in Sensor Networks. 136–148.
- [24] Hongbo Jiang, Chao Cai, Xiaoqiang Ma, Yang Yang, and Jiangchuan Liu. 2018. Smart home based on WiFi sensing: A survey. IEEE Access 6 (2018), 13317–13325.
- [25] Mohamad Katanbaf, Anthony Weinand, and Vamsi Talla. 2021. Simplifying Backscatter Deployment: Full-Duplex LoRa Backscatter. In 18th USENIX Symposium on Networked Systems Design and Implementation (NSDI 21). USENIX Association, 955–972. https://www.usenix.org/conference/nsdi21/presentation/katanbaf
- [26] Ali Khaleghi, Aminolah Hasanvand, and Ilangko Balasingham. 2018. Radio frequency backscatter communication for high data rate deep implants. IEEE Transactions on Microwave Theory and Techniques 67, 3 (2018), 1093–1106.
- [27] Y.-T. Lin. 2005. Low-power variable-length fast Fourier transform processor. IEE Proceedings - Computers and Digital Techniques 152 (July 2005), 499–506(7). Issue 4. https://digital-library.theiet.org/content/journals/10.1049/ip-cdt_20041224
- [28] Fan Liu, Christos Masouros, Athina P Petropulu, Hugh Griffiths, and Lajos Hanzo. 2020. Joint radar and communication design: Applications, state-of-the-art, and the road ahead. *IEEE Transactions on Communications* 68, 6 (2020), 3834–3862.
- [29] Haofan Lu, Mohammad Mazaheri, Reza Rezvani, and Omid Abari. 2023. A Millimeter Wave Backscatter Network for Two-Way Communication and Localization. In Proceedings of the ACM SIGCOMM 2023 Conference. 49–61.
- [30] Yongsen Ma, Gang Zhou, and Shuangquan Wang. 2019. WiFi sensing with channel state information: A survey. ACM Computing Surveys (CSUR) 52, 3 (2019), 1–36.
- [31] Mohammad Mazaheri, Rafael Ruiz, Domenico Giustiniano, Joerg Widmer, and Omid Abari. 2023. Bringing Millimeter Wave Technology to Any IoT Device. In Proceedings of the 29th Annual International Conference on Mobile Computing and Networking. 1–15.
- [32] Mohammad Hossein Mazaheri, Alex Chen, and Omid Abari. 2021. Mmtag: A millimeter wave backscatter network. In Proceedings of the 2021 ACM SIGCOMM 2021 Conference. 463–474.
- [33] Kang Min Bae, Namjo Ahn, Yoon Chae, Parth Pathak, Sung-Min Sohn, and Song Min Kim. 2024. Omniscatter: Extreme Sensitivity MMWave Backscattering Using Commodity FMCW Radar. GetMobile: Mobile Computing and Communications 27, 4 (2024), 26–30.
- [34] John Nolan, Kun Qian, and Xinyu Zhang. 2021. RoS: passive smart surface for roadside-to-vehicle communication. In Proceedings of the 2021 ACM SIGCOMM 2021 Conference. 165–178.
- [35] Safwat Mostafa Noor, Eugene John, and Manoj Panday. 2019. Design and Implementation of an Ultralow-Energy FFT ASIC for Processing ECG in Cardiac Pacemakers. IEEE Transactions on Very Large Scale Integration (VLSI) Systems 27, 4 (2019), 983–987. https://doi.org/10.1109/TVLSI.2018.2883642
- [36] Kun Qian, Lulu Yao, Xinyu Zhang, and Tse Nga Ng. 2022. MilliMirror: 3D printed reflecting surface for millimeter-wave coverage expansion. In Proceedings of the 28th Annual International Conference on Mobile Computing And Networking. 15–28.
- [37] Kun Qian, Lulu Yao, Kai Zheng, Xinyu Zhang, and Tse Nga Ng. 2023. UniScatter: a Metamaterial Backscatter Tag for Wideband Joint Communication and Radar

- Sensing. In Proceedings of the 29th Annual International Conference on Mobile Computing and Networking. 1–16.
- [38] Siji Quan, Weiping Qian, Junhai Guq, and Van Zhang. 2014. Radar-communication integration: An overview. In The 7th IEEE/International Conference on Advanced Infocomm Technology. IEEE, 98–103.
- [39] Barry J Rubin and Bhupindra Singh. 2000. Study of meander line delay in circuit boards. IEEE Transactions on microwave theory and techniques 48, 9 (2000), 1452– 1460.
- [40] Cenk Sahin, John Jakabosky, Patrick M. McCormick, Justin G. Metcalf, and Shannon D. Blunt. 2017. A novel approach for embedding communication symbols into physical radar waveforms. In 2017 IEEE Radar Conference (RadarConf). 1498–1503. https://doi.org/10.1109/RADAR.2017.7944444
- [41] Elahe Soltanaghaei, Adwait Dongare, Akarsh Prabhakara, Swarun Kumar, Anthony Rowe, and Kamin Whitehouse. 2021. Tagfi: Locating ultra-low power wifitags using unmodified wifi infrastructure. Proceedings of the ACM on Interactive, Mobile, Wearable and Ubiquitous Technologies 5, 1 (2021), 1–29.
- [42] Elahe Soltanaghaei, Avinash Kalyanaraman, and Kamin Whitehouse. 2017. Peripheral wift vision: Exploiting multipath reflections for more sensitive human sensing. In Proceedings of the 4th International on Workshop on Physical Analytics. 13–18.
- [43] Elahe Soltanaghaei, Avinash Kalyanaraman, and Kamin Whitehouse. 2018. Multi-path triangulation: Decimeter-level wifi localization and orientation with a single unaided receiver. In Proceedings of the 16th annual international conference on mobile systems, applications, and services. 376–388.
- [44] Elahe Soltanaghaei, Akarsh Prabhakara, Artur Balanuta, Matthew Anderson, Jan M Rabaey, Swarun Kumar, and Anthony Rowe. 2021. Millimetro: mmWave retro-reflective tags for accurate, long range localization. In Proceedings of the 27th Annual International Conference on Mobile Computing and Networking. 69–82.
- [45] Elahe Soltanaghaei, Rahul Anand Sharma, Zehao Wang, Adarsh Chittilappilly, Anh Luong, Eric Giler, Katie Hall, Steve Elias, and Anthony Rowe. 2020. Robust and practical WiFi human sensing using on-device learning with a domain

- adaptive model. In Proceedings of the 7th ACM International Conference on Systems for Energy-Efficient Buildings, Cities, and Transportation. 150–159.
- [46] Sheng Tan, Yili Ren, Jie Yang, and Yingying Chen. 2022. Commodity WiFi Sensing in Ten Years: Status, Challenges, and Opportunities. *IEEE Internet of Things Journal* 9, 18 (2022), 17832–17843.
- [47] Christiana Varnava. 2021. Radar in a phone. Nature Electronics 4, 3 (2021), 173–173.
- [48] Ambuj Varshney, Oliver Harms, Carlos Perez Penichet, Christian Rohner, Frederik Hermans, and Thiemo Voigt. 2017. LoRea: A Backscatter Architecture that Achieves a Long Communication Range. arXiv:1611.00096 [cs.NI]
- [49] Deepak Vasisht, Guo Zhang, Omid Abari, Hsiao-Ming Lu, Jacob Flanz, and Dina Katabi. 2018. In-body backscatter communication and localization. In Proceedings of the 2018 Conference of the ACM Special Interest Group on Data Communication (Budapest, Hungary) (SIGCOMM '18). Association for Computing Machinery, New York, NY, USA, 132–146. https://doi.org/10.1145/3230543.3230565
- [50] Xuan Wang, Xin Kou, Haoyu Li, Fuwei Wang, Dingyi Fang, Yunfei Ma, and Xiaojiang Chen. 2022. AllSpark: Enabling Long-Range Backscatter for Vehicleto-Infrastructure Communication. *IEEE Internet of Things Journal* 9, 24 (2022), 25525–25537.
- [51] Timothy Woodford, Kun Qian, and Xinyu Zhang. 2023. Metasight: High-Resolution NLoS Radar Sensing through Efficient Metasurface Encoding. (2023).
- [52] Zhifan Ye, Zhengchun Zhou, Pingzhi Fan, Zilong Liu, Xianfu Lei, and Xiaohu Tang. 2022. Low ambiguity zone: Theoretical bounds and Doppler-resilient sequence design in integrated sensing and communication systems. *IEEE Journal on Selected Areas in Communications* 40, 6 (2022), 1809–1822.
- [53] Hongxi Zhang and Pei Wang. 2022. An Improved 3D Ultra-Wideband High-Efficiency Substrate Integrated Coaxial Meander Delay Line. *Electronics* 11, 23 (2022), 3869.
- [54] Yutian Zhao, A.T. Erdogan, and T. Arslan. 2005. A novel low-power reconfigurable FFT processor. In 2005 IEEE International Symposium on Circuits and Systems (ISCAS). 41–44 Vol. 1. https://doi.org/10.1109/ISCAS.2005.1464519